

Isoscalar monopole and dipole excitations of cluster states and giant resonances in ^{12}C

Yoshiko Kanada-En'yo

Department of Physics, Kyoto University, Kyoto 606-8502, Japan

The isoscalar monopole(ISM) and dipole(ISD) excitations in ^{12}C are theoretically investigated with the shifted antisymmetrized molecular dynamics(AMD) plus 3α -cluster generator coordinate method(GCM). The small amplitude vibration modes are described by coherent one-particle one-hole excitations expressed by small shift of single-nucleon Gaussian wave functions within the AMD framework, whereas the large amplitude cluster modes are incorporated by superposing 3α -cluster wave functions in the GCM. The coupling of the excitations in the intrinsic frame with the rotation and parity transformation is taken into account microscopically by the angular-momentum and parity projections. The present calculation describes the ISM and ISD excitations in a wide energy region covering cluster modes in the low-energy region and the giant resonances in the high-energy region, though the quantitative description of the high-energy part is not satisfactory. The low-energy ISM and ISD strengths of the cluster modes are enhanced by the radial motion of α clusters, and they split into a couple of states because of the angular motion of α clusters. The low-energy ISM strengths exhaust 26% of the EWSR, which is consistent with the experimental data for the $^{12}\text{C}(0_2^+; 7.65 \text{ MeV})$ and $^{12}\text{C}(0_3^+; 10.3 \text{ MeV})$ measured by (e, e') , (α, α') , and $({}^6\text{Li}, {}^6\text{Li}')$ scatterings. In the calculated low-energy ISD strengths, two 1^- states (the 1_1^- and 1_2^-) with the significant strengths are obtained in $E = 10 - 15 \text{ MeV}$. It is indicated that the ISD excitations can be a good probe to experimentally search for new cluster states such as the $^{12}\text{C}(1_2^-)$ obtained in the present calculation.

I. INTRODUCTION

Isoscalar monopole(ISM) and dipole(ISD) strength distributions measured by hadron inelastic scattering experiments have been providing useful informations for nuclear properties concerning nuclear excitations corresponding to the compressional vibration modes as well as the nuclear matter incompressibility. Isoscalar giant monopole resonances(ISGMRs), which were established in medium and heavy nuclei [1–4], have been studied extensively between ^{12}C and ^{206}Pb [5–10]. The ISGMRs in medium and heavy nuclei exhaust almost 100% of the isoscalar monopole(ISM) energy-weighted sum rule(EWSR), and the excitation energies have been used to extract the compressibility of the nuclear matter with microscopic calculations using, for example, non-relativistic and relativistic mean-field approaches and those plus random-phase approximation(RPA) (see Refs. [11–15] and references therein). High precision studies using hadron inelastic scatterings have revealed that the ISM strength distributions in nuclei lighter than ^{40}Ca are strongly fragmented [5–7, 9, 10]. In the ISM strengths in ^{16}O , the significant percentage of the EWSR has been found in a low-energy region. In the theoretical study of ^{16}O with a 4α calculation by Yamada *et al.*, it was pointed out that two different types of ISM excitations exist in ^{16}O [16]: the low-energy ISM strengths of cluster excitations in $E \lesssim 16 \text{ MeV}$ are separated from the high-energy ISM strengths of the ISGMR in $E > 16 \text{ MeV}$, which correspond to the collective vibration mode described by coherent one-particle and one-hole (1p-1h) excitations in a mean field. The separation of the low-energy ISM strengths from the ISGMR was also found in ^{12}C [5, 9]. The ISM strength distributions in ^{12}C observed by (α, α') and $({}^6\text{Li}, {}^6\text{Li}')$ scatterings [5, 9, 17] show that the low-energy ISM strengths in $E \lesssim 12 \text{ MeV}$ exhaust the significant percentage of the EWSR comparable to the high-energy strengths in $E > 12 \text{ MeV}$ of the ISGMR. In ^{12}C , a couple of excited 0^+ states have been experimentally observed near the 3α threshold energy (see, for instance, Refs. [9, 18, 19] and references therein). Theoretically, these states are considered to be 3α -cluster states [20–38]. The remarkable E0 strength for the 0_2^+ (7.65 MeV) state was observed by electron scattering [39, 40], and the inelastic form factor for the 0_2^+ is described well by 3α -cluster models [21, 23, 32, 36]. In general, the ISM strengths can be strongly concentrated on cluster states in the low-energy region because the ISM operator directly excites the cluster motion with $L = 0$ as well as the compressional monopole vibration mode [16]. Therefore, the low-energy ISM strengths separating from the ISGMR is a good probe to study cluster states in light nuclei as discussed for ^{12}C , ^{16}O , ^{11}B , and ^{24}Mg [16, 35, 41–46].

In analogy to the ISM excitations, the ISD excitations can be another probe to search for cluster states because the ISD operator is able to excite the cluster motion with $L = 1$ as well as the compressional dipole vibration mode. The isoscalar giant dipole resonances (ISGDRs) observed by (α, α') scatterings are found generally in the higher energy region than the ISGMR (see Refs. [15, 47–49] and references therein). Compared with the ISM strength distributions, the observed ISD strengths in medium and heavy nuclei are strongly fragmented and concentrate typically in two bump structures [50, 51]: one in the low-energy region and the other in the relatively higher energy region, which are considered to correspond to the toroidal dipole mode and the compressional dipole vibration mode, respectively [15, 49, 52–55]. In ^{16}O and ^{40}Ca , the low-energy ISD strengths concentrate on the 1^- states at $E = 7.12 \text{ MeV}$ and

$E = 6.95$ MeV, respectively, which exhaust approximately 4% of the EWSR [48, 56]. Also in ^{12}C , the significant low-energy ISD strengths have been observed in $E \leq 20$ MeV below the high-energy strengths of the ISGDR [9]. The separation of the low-energy ISD strengths from the high-energy strengths of the ISGDR for the compressional dipole vibration mode suggests two different types of ISD modes. In the case of light nuclei, the low-energy ISD strengths could correspond to the cluster excitations.

The aim of this paper is to investigate ISM and ISD excitations in ^{12}C from low-energy to high-energy regions and to clarify the separation of the cluster excitations from the ISGMR and ISGDR for the collective vibration modes. In the history of theoretical studies of the giant resonances, RPA calculations in mean-field approaches have been widely applied. Although the RPA calculations are successful for a variety of collective excitations in heavy mass nuclei, the RPA is not useful to describe well-developed cluster states and fails to reproduce the low-energy ISM strengths in ^{16}O [7, 58] because it is a small amplitude approach and unable to describe the large amplitude cluster motions. Moreover, in most of current mean-field approaches, calculations are based a parity-symmetric mean field in a strong coupling picture without the angular-momentum and parity projections, and the coupling of single-particle excitations in the mean-field with the rotation and parity transformation is not taken into account microscopically. The ISM transitions to the 0^+ states having 3α -cluster structures near and above the 3α threshold have been theoretically investigated by microscopic and semi-microscopic 3α -cluster models [21, 23, 32, 35] as well as other structure models such as the antisymmetrized molecular dynamics (AMD) [33] and fermionic molecular dynamics (FMD) [36] and also the *ab initio* calculation [59]. However, these calculations have not yet been applied to investigate the relatively high-energy ISGMR and ISGDR strengths for the collective vibration modes contributed by coherent 1p-1h excitations.

To take into account the large amplitude cluster modes and the coherent 1p-1h excitations as well as the angular-momentum and parity projections, I have recently developed the AMD method [60–63] in Refs. [64, 65]. The applications of the AMD to collective vibration modes go back to the works on electric dipole (E1) and ISM excitations [66, 67] with the time-dependent AMD, which was originally developed for study of heavy-ion reactions [68, 69]. However, in the time-dependent AMD approach, the angular-momentum and parity projections are not performed. Instead of the time-dependent AMD, we superpose the angular-momentum and parity projected wave functions of various configurations including the 1p-1h and cluster excitations. I first perform the variation after the angular-momentum and parity projections in the AMD framework (AMD+VAP) to obtain the ground state wave function of ^{12}C as done in Refs. [25, 33]. Then I describe small amplitude motions by taking into account 1p-1h excitations on the obtained ground state wave function with the shifted AMD method [64, 65]. To incorporate the large amplitude cluster motions, I combine the the generator coordinate method (GCM) with the shifted AMD by superposing 3α -cluster wave functions. The angular-momentum and parity projections are performed in the present framework. Applying the present method, I investigate the ISM and ISD excitations in ^{12}C .

This paper is organized as follows. The present method is formulated in section II, and section III discusses the ground state structure and the ISM and ISD excitations in ^{12}C . The paper concludes with a summary in section IV.

II. FORMULATIONS OF SHIFTED AMD AND 3α -CLUSTER GCM FOR ISM AND ISD EXCITATIONS

In order to calculate the ISM and ISD excitations in ^{12}C , I apply the shifted AMD based on the AMD+VAP and combine it with the 3α -cluster GCM. In this section, I explain the formulations of the AMD+VAP, the shifted AMD, and the 3α -cluster GCM, and also describe the definitions of the ISM and ISD transitions. For the details of the AMD method, the reader is referred to Refs. [62, 63] and references therein.

A. AMD wave function

An AMD wave function is given by a Slater determinant,

$$\Phi_{\text{AMD}}(\mathbf{Z}) = \frac{1}{\sqrt{A!}} \mathcal{A}\{\varphi_1, \varphi_2, \dots, \varphi_A\}, \quad (1)$$

where \mathcal{A} is the antisymmetrizer. The i th single-particle wave function φ_i is written by a product of spatial, spin, and isospin wave functions as

$$\varphi_i = \phi_{\mathbf{X}_i} \chi_i \tau_i, \quad (2)$$

$$\phi_{\mathbf{X}_i}(\mathbf{r}_j) = \left(\frac{2\nu}{\pi}\right)^{4/3} \exp\{-\nu(\mathbf{r}_j - \mathbf{X}_i)^2\}, \quad (3)$$

$$\chi_i = \left(\frac{1}{2} + \xi_i\right)\chi_{\uparrow} + \left(\frac{1}{2} - \xi_i\right)\chi_{\downarrow}. \quad (4)$$

$\phi_{\mathbf{X}_i}$ and χ_i are the spatial and spin functions, respectively, and τ_i is the isospin function fixed to be up (proton) or down (neutron). The width parameter ν is fixed to be the optimized value. To separate the center of mass motion from the total wave function $\Phi_{\text{AMD}}(\mathbf{Z})$, the following condition should be satisfied,

$$\frac{1}{A} \sum_{i=1, \dots, A} \mathbf{X}_i = 0. \quad (5)$$

In the present calculation, I keep this condition and exactly remove the contribution of the center of mass motion. Accordingly, an AMD wave function is expressed by a set of variational parameters, $\mathbf{Z} \equiv \{\mathbf{X}_1, \dots, \mathbf{X}_A, \xi_1, \dots, \xi_A\}$, which specify centroids of single-nucleon Gaussian wave packets and spin orientations for all nucleons. It should be commented that the AMD wave function is similar to the wave function used in FMD calculations [70, 71].

In the AMD framework, existence of clusters is not assumed *a priori* because Gaussian centroids, $\mathbf{X}_1, \dots, \mathbf{X}_A$, of all single-nucleon wave packets are independently treated as variational parameters. Nevertheless, a multi-center cluster wave function can be described by the AMD wave function with the corresponding configuration of Gaussian centroids. It should be also commented that, when all $|\mathbf{X}_i|$ goes to the small limit, the AMD wave function is equivalent to a shell-model configuration because of the mathematical consequence of the antisymmetrized Gaussian wave packets.

B. AMD+VAP

To obtain the ground state wave function of an A -nucleon system, the AMD+VAP method is applied. In the AMD+VAP method, the parameters $\mathbf{Z} = \{\mathbf{X}_1, \mathbf{X}_2, \dots, \mathbf{X}_A, \xi_1, \xi_2, \dots, \xi_A\}$ in the AMD wave function are determined by the energy variation after the angular-momentum and parity projections (VAP). It means that \mathbf{X}_i and ξ_i for the lowest J^π state are optimized so as to minimize the energy expectation value of the Hamiltonian for the J^π -projected AMD wave function;

$$\frac{\delta}{\delta \mathbf{X}_i} \frac{\langle \Phi | H | \Phi \rangle}{\langle \Phi | \Phi \rangle} = 0, \quad (6)$$

$$\frac{\delta}{\delta \xi_i} \frac{\langle \Phi | H | \Phi \rangle}{\langle \Phi | \Phi \rangle} = 0, \quad (7)$$

$$\Phi = P_{MK}^{J^\pi} \Phi_{\text{AMD}}(\mathbf{Z}), \quad (8)$$

where $P_{MK}^{J^\pi}$ is the angular-momentum and parity projection operator. After the VAP calculation with $J^\pi = 0^+$, the optimized parameters $\mathbf{Z}^0 = \{\mathbf{X}_1^0, \dots, \xi_1^0, \dots\}$ for the ground state of ^{12}C are obtained.

C. Shifted AMD

To incorporate 1p-1h excitations, I consider small variation $\delta\varphi_i$ of the single-particle wave function φ_i in the ground state wave function $\Phi_{\text{AMD}}(\mathbf{Z}^0)$ by shifting the position of the Gaussian centroid, $\mathbf{X}_i^0 \rightarrow \mathbf{X}_i^0 + \Delta_\sigma$, where Δ_σ is the small vector specified by the label σ for the shift direction. In the present calculation, 8 directions ($\sigma = 1, \dots, 8$) are adopted to obtain the approximately converged result for the ISM and ISD strengths. I choose enough small shift, typically $\Delta = |\Delta_\sigma| = 0.1 \sim 0.2$ fm, so as to obtain Δ -independent results. Details of the adopted $\Delta_{\sigma=1, \dots, 8}$ are described in section III. For the spin part, I consider the spin-nonflip single-particle state χ_i and the spin-flip state $\bar{\chi}_i$ ($\langle \bar{\chi}_i | \chi_i \rangle = 0$);

$$\bar{\chi}_i = \left(\frac{1}{2} + \bar{\xi}_i\right)\chi_\uparrow + \left(\frac{1}{2} - \bar{\xi}_i\right)\chi_\downarrow, \quad (9)$$

where $\bar{\xi}_i = -1/4\xi_i^*$. For all single-particle wave functions, I consider spin-nonflip and spin-flip states shifted to 8 directions ($\Delta_{\sigma=1, \dots, 8}$) independently and prepare $16A$ AMD wave functions, $\Phi_{\text{AMD}}(\mathbf{Z}_{\text{nonflip}}^0(i, \sigma))$ and $\Phi_{\text{AMD}}(\mathbf{Z}_{\text{flip}}^0(i, \sigma))$ with the parameters,

$$\mathbf{Z}_{\text{nonflip}}^0(i, \sigma) \equiv \{\mathbf{X}_1^{0'}, \dots, \mathbf{X}_i^{0'} + \Delta_\sigma, \dots, \mathbf{X}_A^{0'}, \xi_1^0, \dots, \xi_i^0, \dots, \xi_A^0\}, \quad (10)$$

$$\mathbf{Z}_{\text{flip}}^0(i, \sigma) \equiv \{\mathbf{X}_1^{0'}, \dots, \mathbf{X}_i^{0'} + \Delta_\sigma, \dots, \mathbf{X}_A^{0'}, \xi_1^0, \dots, \bar{\xi}_i^0, \dots, \xi_A^0\}, \quad (11)$$

where $\mathbf{X}_j^{0'} = \mathbf{X}_j^0 - \Delta_\sigma/(A-1)$ to take into account the recoil effect so that the center of mass motion is separated exactly. Those shifted AMD wave functions $\Phi_{\text{AMD}}(\mathbf{Z}_{\text{nonflip}}^0(i, \sigma))$ and the original wave function $\Phi_{\text{AMD}}(\mathbf{Z}^0)$ are superposed to obtain the final wave functions for the ground and excited states,

$$\begin{aligned} \Psi_{12C(J_k^\pi)}^{\text{sAMD}} &= \sum_K c_0(J_k^\pi; K) P_{MK}^{J\pi} \Phi_{\text{AMD}}(\mathbf{Z}^0) \\ &+ \sum_{i=1, \dots, A} \sum_{\sigma} \sum_K c_1(J_k^\pi; i, \sigma, K) P_{MK}^{J\pi} \Phi_{\text{AMD}}(\mathbf{Z}_{\text{nonflip}}^0(i, \sigma)) \\ &+ \sum_{i=1, \dots, A} \sum_{\sigma} \sum_K c_2(J_k^\pi; i, \sigma, K) P_{MK}^{J\pi} \Phi_{\text{AMD}}(\mathbf{Z}_{\text{flip}}^0(i, \sigma)), \end{aligned} \quad (12)$$

where the coefficients c_0 , c_1 , and c_2 are determined by diagonalization of the norm and Hamiltonian matrices. I call this method “the shifted AMD” (sAMD).

The model space of the sAMD contains the 1p-1h excitations that are written by the small shift of single-nucleon Gaussian wave functions of the ground state wave function. In the intrinsic frame before the angular-momentum and parity projections, the ground state AMD wave function is expressed by a Slater determinant, and therefore, the sAMD method corresponds to the RPA in the restricted model space of the linear combination of the shifted Gaussian wave functions. However, since the J^π -projected wave functions are superposed in the sAMD, the coupling of the 1p-1h excitations with the rotation and parity transformation is taken into account microscopically. Moreover, the original wave function for the ground state is the one obtained by the variation after the angular-momentum and parity projections as mentioned previously. It means that the sAMD may contain, in principle, higher correlations beyond the RPA.

D. 3α -cluster GCM

To incorporate the large amplitude α -cluster motions, I combine the 3α -cluster GCM(3α GCM) with the sAMD. In the 3α GCM, I superpose the 3α -cluster wave functions projected from the Brink-Bloch 3α -cluster wave functions [72],

$$\Phi_{3\alpha} = \frac{1}{\sqrt{A!}} \mathcal{A} \{ \Phi_\alpha(\mathbf{R}_1) \Phi_\alpha(\mathbf{R}_2) \Phi_\alpha(\mathbf{R}_3) \}, \quad (13)$$

where $\Phi_\alpha(\mathbf{R}_i)$ is the α -cluster wave function written by the harmonic oscillator ($0s$)⁴ configuration located at \mathbf{R}_i with the width $b = 1/\sqrt{2\nu}$, and \mathbf{R}_i satisfies the relation $\mathbf{R}_1 + \mathbf{R}_2 + \mathbf{R}_3 = 0$. Note that $\Phi_{3\alpha}(\mathbf{R}_1, \mathbf{R}_2, \mathbf{R}_3)$ can be expressed by the AMD wave function with the specific configuration. To taken into account various 3α configurations, the distances $d = |\mathbf{R}_1 - \mathbf{R}_2|$ and $D = |\mathbf{R}_3 - (\mathbf{R}_1 + \mathbf{R}_2)/2|$, and the angle θ between \mathbf{R}_3 and $\mathbf{R}_1 - \mathbf{R}_2$ are treated as generator coordinates in the GCM calculation (see Fig. 1(a)). Then, I combine the 3α GCM with the sAMD and express the total wave function as

$$\begin{aligned} \Psi_{12C(J_k^\pi)}^{\text{sAMD}+3\alpha\text{GCM}} &= \sum_K c_0(J_k^\pi; K) P_{MK}^{J\pi} \Phi_{\text{AMD}}(\mathbf{Z}^0) \\ &+ \sum_{i=1, \dots, A} \sum_{\sigma} \sum_K c_1(J_k^\pi; i, \sigma, K) P_{MK}^{J\pi} \Phi_{\text{AMD}}(\mathbf{Z}_{\text{nonflip}}^0(i, \sigma)) \\ &+ \sum_{i=1, \dots, A} \sum_{\sigma} \sum_K c_2(J_k^\pi; i, \sigma, K) P_{MK}^{J\pi} \Phi_{\text{AMD}}(\mathbf{Z}_{\text{flip}}^0(i, \sigma)) \\ &+ \sum_{d, D, \theta} \sum_K c_3(J_k^\pi; d, D, \theta, K) P_{MK}^{J\pi} \Phi_{3\alpha}(d, D, \theta), \end{aligned} \quad (14)$$

where the coefficients are determined by diagonalization of the norm and Hamiltonian matrices. The summation for three parameters d , D , θ corresponds to the 3α GCM with full 3α configurations, which I call the 3α GCM(full) in the present paper. To see the effect of the angular motion of α clusters, I also perform the 3α GCM calculation with the fixed angle $\theta = \pi/2$ considering only the radial motion with the generator coordinates d and D (see Fig. 1(b)), which I call 3α GCM(radial).

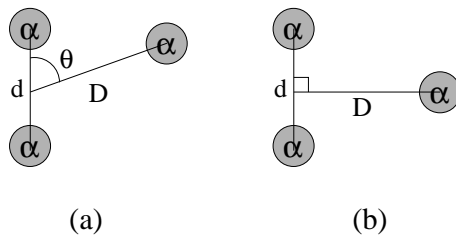


FIG. 1: Schematic figures of 3α configurations for (a) the $3\alpha\text{GCM}(\text{full})$ with the generator coordinates d , D , and θ , and (b) the $3\alpha\text{GCM}(\text{radial})$ with the generator coordinates d and D , and the fixed $\theta = \pi/2$.

E. Isoscalar monopole and dipole transitions

The ISM and ISD operators $\mathcal{M}(\text{IS0})$ and $\mathcal{M}(\text{IS1}; \mu)$, which excite the compressional monopole and dipole modes, respectively, are defined as

$$\mathcal{M}(\text{IS0}) = \sum_i r_{i,\text{in}}^2, \quad (15)$$

$$\mathcal{M}(\text{IS1}; \mu) = \sum_i r_{i,\text{in}}^3 Y_\mu^1(\hat{r}_{i,\text{in}}), \quad (16)$$

where $r_{i,\text{in}}$ is the i th nucleon coordinate with respect to the center of mass. The ISM strength for $0_1^+ \rightarrow 0_k^+$ and the ISD strength for $0_1^+ \rightarrow 1_k^-$ are given by the reduced matrix elements of these operators as

$$B(\text{IS0}; 0_1^+ \rightarrow 0_k^+) = \frac{1}{2J_{\text{g.s.}} + 1} |\langle 0_k^+ | \mathcal{M}(\text{IS0}) | 0_1^+ \rangle|^2, \quad (17)$$

$$B(\text{IS1}; 0_1^+ \rightarrow 1_k^-) = \frac{1}{2J_{\text{g.s.}} + 1} |\langle 1_k^- | \mathcal{M}(\text{IS1}) | 0_1^+ \rangle|^2, \quad (18)$$

where $J_{\text{g.s.}}$ is the ground state angular momentum, and in the present case it is zero. The energy-weighted sum (EWS) of the strengths is given as

$$S(\text{IS0}) \equiv \sum_{k \geq 2} E_{0_k^+} B(\text{IS0}; 0_1^+ \rightarrow 0_k^+), \quad (19)$$

$$S(\text{IS1}) \equiv \sum_{k \geq 1} E_{1_k^-} B(\text{IS1}; 0_1^+ \rightarrow 1_k^-). \quad (20)$$

If the interaction commutes with the ISM operator, the ISM energy weighted sum rule (EWSR) is given as

$$S(\text{IS0}) = \frac{2\hbar^2}{m} \langle 0_1^+ | \sum_i r_{i,\text{in}}^2 | 0_1^+ \rangle = \frac{2\hbar^2}{m} A \langle r^2 \rangle_{\text{g.s.}}, \quad (21)$$

where $\langle r^2 \rangle_{\text{g.s.}}$ is the mean-square radius of the ground state.

III. RESULTS

A. Effective nuclear interactions

I use an effective nuclear interaction consisting of the central force of the MV1 force (case 3)[73] and the spin-orbit force of the G3RS force [74, 75], and the Coulomb force. The MV1 force consists of a two-range Gaussian two-body term and a zero-range three-body term. The G3RS spin-orbit force is a two-range Gaussian force. The Bartlett, Heisenberg, and Majorana parameters, $b = h = 0$ and $m = 0.62$, in the MV1 force are adopted, and the strengths $u_I = -u_{II} \equiv u_{Is} = 3000$ MeV of the G3RS spin-orbit force is used. These interaction parameters are the same as those used in Refs. [25, 33], in which the AMD+VAP calculation describes properties of the ground and excited states in $E \lesssim 15$ MeV of ^{12}C .

B. Parameter setting and the ground state of ^{12}C

The width parameter $\nu = 0.19 \text{ fm}^{-2}$ is chosen for the AMD wave function so as to minimize the ground state energy of ^{12}C calculated by the AMD+VAP.

In the sAMD, I try three sets of vectors, $\Delta_{\sigma=x,y,z} = \epsilon(1, 0, 0), \epsilon(0, 1, 0), \epsilon(0, 0, 1)$, $\Delta_{\sigma=1,\dots,8} = \epsilon(\pm 1, \pm 1, \pm 1)$, $\Delta_{\sigma=1,\dots,14} = \epsilon(\pm 1, \pm 1, \pm 1), (\pm 1, 0, 0), (0, \pm 1, 0), (0, 0, \pm 1)$ for the shift of Gaussian centroids, and check the convergence of the ISM and ISD strengths on the number of the directions σ . Here, ϵ is chosen to be 0.1 fm which is small enough to give the ϵ -independent result. The x , y , and z axes are chosen to be the principle axes of the inertia in the intrinsic frame and satisfy $\langle x^2 \rangle \leq \langle y^2 \rangle \leq \langle z^2 \rangle$ and $\langle xy \rangle = \langle yz \rangle = \langle zx \rangle = 0$ for the intrinsic wave function $\Phi_{\text{AMD}}(\mathbf{Z}^0)$. The ISM and ISD strengths calculated by the sAMD with three choices, $e_{\sigma=x,y,z}$, $e_{\sigma=1,\dots,8}$, and $e_{\sigma=1,\dots,14}$, are shown in Fig. 2, which shows the strength distributions smeared by a Gaussian with the width $\gamma = 2 \text{ MeV}$. It is found that the set $\Delta_{\sigma=1,\dots,8}$ is practically enough to get an approximately converged result for both the ISM and ISD strengths, whereas $\Delta_{\sigma=x,y,z}$ is enough only for the ISM strengths but not for the ISD strengths. I adopt the set $\Delta_{\sigma=1,\dots,8}$ in the present sAMD+3 α GCM calculation.

For the generator coordinates in the 3 α GCM, $d = 1.8 + n_d \text{ fm}$ ($n_d = 0, \dots, 4$) and $D = 2 + n_D \text{ fm}$ ($n_D = 0, \dots, 5$) are adopted in the 3 α GCM(full) and 3 α GCM(radial). In addition, $\theta = \pi n_\theta / 8$ ($n_\theta = 0, \dots, 4$) are used in the 3 α GCM(full).

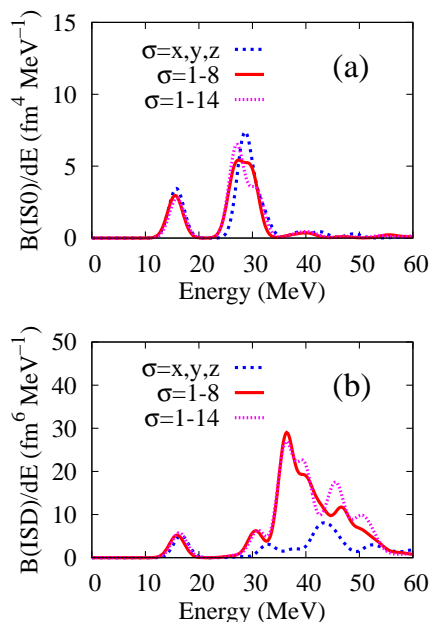


FIG. 2: (color online) (a) ISM and (b) ISD strength distributions of ^{12}C calculated by the sAMD with $e_{\sigma=x,y,z}$, $e_{\sigma=1,\dots,8}$, and $e_{\sigma=1,\dots,14}$. The strengths are smeared by a Gaussian with the width $\gamma = 2 \text{ MeV}$.

C. Ground state structure

The wave function $\Phi_{\text{AMD}}(\mathbf{Z}^0)$ obtained by the AMD+VAP for the ground state contains the α cluster correlation as well as the $p_{3/2}$ -closed configuration as discussed in Refs. [25, 33]. As seen in the density distribution in Fig. 3, the intrinsic wave function of the ground state has a triaxial deformation with the cluster structure. In the sAMD and sAMD+3 α GCM(full) calculations, the ground state wave function is expressed by the linear combination of many configurations as given in Eqs. (12) and (14), however, it is still dominated by $P_{00}^{0+} \Phi_{\text{AMD}}(\mathbf{Z}^0)$ with 96% (91%) in the sAMD(sAMD+3 α GCM(full)). The calculated binding energy (B.E.) and root-mean-square matter radius (r_m) of ^{12}C calculated by the AMD+VAP, sAMD, and sAMD+3 α GCM(full) are B.E. = 86.7 MeV, 89.0 MeV, 89.6 MeV, and $r_m = 2.41 \text{ fm}$, 2.41 fm, and 2.46 fm, respectively, which reasonably agree to the experimental values B.E. = 92.16 MeV and $r_p = 2.33 \text{ fm}$ (the point-proton radius) reduced from the charge radius [76].

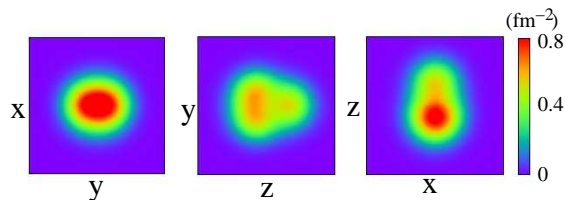


FIG. 3: (color online) Density distribution of the intrinsic wave function of the ^{12}C ground state obtained by the AMD+VAP. The density is projected onto the xy (left), yz (middle), and zx (right) planes.

D. ISM strengths

The ISM strengths for $0_1^+ \rightarrow 0_k^+$ ($k \geq 2$) obtained by the sAMD, sAMD+3 α GCM(radial), and sAMD+3 α GCM(full) are shown in Fig. 4. In the sAMD, sAMD+3 α GCM(radial), and sAMD+3 α GCM(full) results, the total energy weighted sum (TEWS) of the ISM strengths corresponds to 97%, 100%, and 100% of the EWSR in Eq. (21), respectively. In the three calculations, the remarkable ISM strengths exist in $E = 25 - 30$ MeV corresponding to the ISGMR. In the sAMD result (Fig. 4(a)), a low-energy ISM resonance is found at $E \sim 15$ MeV and regarded as a signal of the cluster excitation. As seen in the sAMD+3 α GCM(radial) result (Fig. 4(b)), this low-energy mode comes down below $E = 10$ MeV, and its ISM strength is remarkably enhanced by the large amplitude radial motion of α clusters. It should be noted that a part of the ISGMR strength feeds the low-energy strength. Furthermore, in the sAMD+3 α GCM(full) calculation with the radian and angular motions of α clusters, the low-energy mode splits into two states around $E = 10$ MeV (see Fig. 4(c)).

The lower state is assigned to the experimentally known 0_2^+ state at 7.65 MeV. The calculated $B(\text{IS0})$ agrees well to the experimental value $B(\text{IS0}) = 120 \pm 4 \text{ fm}^4$ evaluated from the E0 strength measured by electron scatterings [40] as $B(\text{IS0}) = 4B(\text{E0})$ assuming the isospin symmetry. The higher state corresponds to the 0_3^+ state predicted by the AMD and FMD calculations [25, 28, 33, 36] as well as the 3 α -cluster calculations [22, 34]. The sum of the ISM strengths of the two 0^+ states (0_2^+ and 0_3^+) in the sAMD+3 α GCM(full) is almost the same as the ISM strength of the low-energy mode obtained by the sAMD+3 α GCM(radial). Namely, the low-energy mode with the remarkable ISM strength arises from the radial excitation of α clusters, and its strength is dominantly carried by the 0_2^+ and partly shared by the 0_3^+ state. In the comparison of the ISM strengths between the sAMD, sAMD+3 α GCM(radial), and sAMD+3 α GCM(full) results, it is found that the enhancement and splitting of the low-energy ISM strengths occur from the radial and angular motions of α clusters, respectively.

E. ISD strengths

The ISD strengths for $0_1^+ \rightarrow 1_k^-$ ($k \geq 1$) calculated by the sAMD, sAMD+3 α GCM(radial), and sAMD+3 α GCM(full) are shown in Fig. 5. Interestingly, also in the ISD strengths, the enhancement and splitting of the low-energy strengths occur from the radial and angular motions of α clusters, respectively. The ISGDR is found in the energy $E = 30 - 55$ MeV region higher than the ISGMR energy. These high-energy strengths for the ISGDR are not so affected by the large amplitude cluster motions. Below the ISGDR, the sAMD result shows a low-energy ISD resonance at $E \sim 15$ MeV regarded as a signal of the cluster mode. The low-energy ISD strength of the cluster mode is enhanced about twice by the radial motion of α clusters in the sAMD+3 α GCM(radial) result, and it splits into at least two states in $E = 10 - 15$ MeV because of the angular motion of α clusters in the sAMD+3 α GCM(full) result. Consequently, the low-energy ISD strengths of the cluster mode are shared by the two states almost equally. The lower state can be assigned to the experimentally known 1_1^- state at 10.84 MeV. For the higher 1^- state, there is no corresponding state confirmed experimentally, however, the significant ISD strengths around $E = 15$ MeV have been observed by (α, α') scatterings and could be a signal of the higher 1^- state obtained in the present calculation. More details are discussed later.

F. Energy weighted strength distributions

The energy weighted ISM and ISD strength distributions calculated by the sAMD+3 α GCM(full) are compared with those measured by (α, α') scatterings [9] in Fig. 6. The calculated high-energy strengths for the ISGMR and

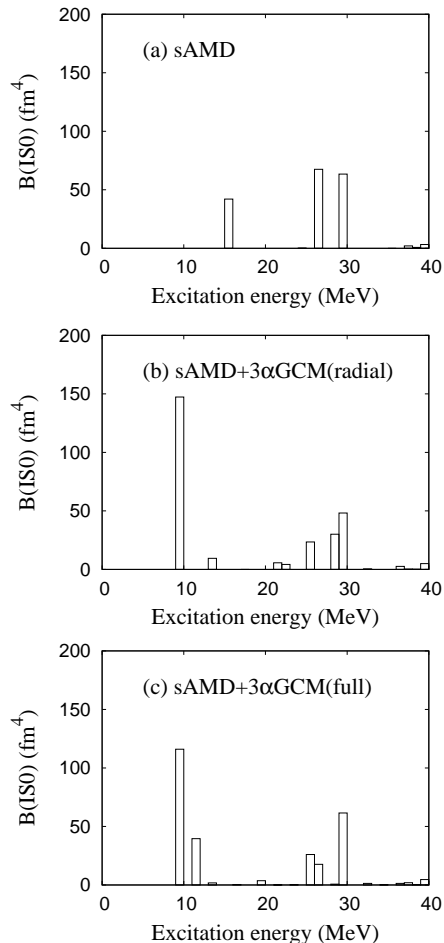


FIG. 4: The ISM strengths calculated by the sAMD, sAMD+3 α GCM(radial), and sAMD+3 α GCM(full). The sum of the strengths $B(\text{ISO})$ in each energy bin is shown.

ISGDR are found around $E = 30$ MeV and $E = 40$ MeV, respectively. The low-energy ISM and ISD strengths for the cluster modes exist in the energy regions much below the giant resonances. The percentages of the strengths in the low-energy and high-energy regions calculated by the sAMD+3 α GCM(full) are shown in Table I, compared with those of the sAMD and sAMD+3 α GCM(radial) calculations.

The low-energy ISM strengths for the 0^+ states around $E = 10$ MeV is only 11% of the EWSR in the sAMD, however, they are largely enhanced by the large amplitude cluster motions and exhaust 26% of the EWSR in the sAMD+3 α GCM(radial) and sAMD+3 α GCM(full). The fact that the sum of the low-energy and high-energy strengths is almost constant (75 – 77 % of the EWSR) in three calculations indicates that the increment of the low-energy ISM strengths come from the ISGMR strength, which originally concentrates in the high-energy region in the sAMD. In other words, in the sAMD calculation without the large amplitude cluster modes, a part of the strengths of the cluster modes is involved by the ISGMR.

The feature of the experimental ISM strength distributions (Fig. 6 (c)) which consists of the high-energy strengths of the ISGMR and the significant low-energy strengths are qualitatively described by the calculation (Fig. 6(a)), however, the quantitative description of the high-energy part is not satisfactory in the present result. The present calculation overestimates the centroid energy (21.9 ± 0.3 MeV) and the strengths ($27 \pm 5\%$ of the EWSR) of the observed ISGMR, and also fails to describe the width of the ISGMR. The present model space of the sAMD is restricted only in the single-particle excitations written by shifted Gaussians and insufficient to describe the spreading width of the ISGMR.

For the low-energy ISM strengths, the calculated strength for the 0_2^+ state exhausts 18% of the EWSR, which well agrees to the experimental values for the 0_2^+ (7.65 MeV), 15% in Ref. [39] and 17% in Ref. [40], measured by (e, e') scatterings (see Fig. 6(a) and Table II). The data evaluated by (α, α') [9] and $({}^6\text{Li}, {}^6\text{Li}')$ [17] scatterings is $7.6 \pm 0.9\%$ and 9.5% , which is about a half of the values measured (e, e') scatterings. This inconsistency of the ISM strength for the 0_2^+

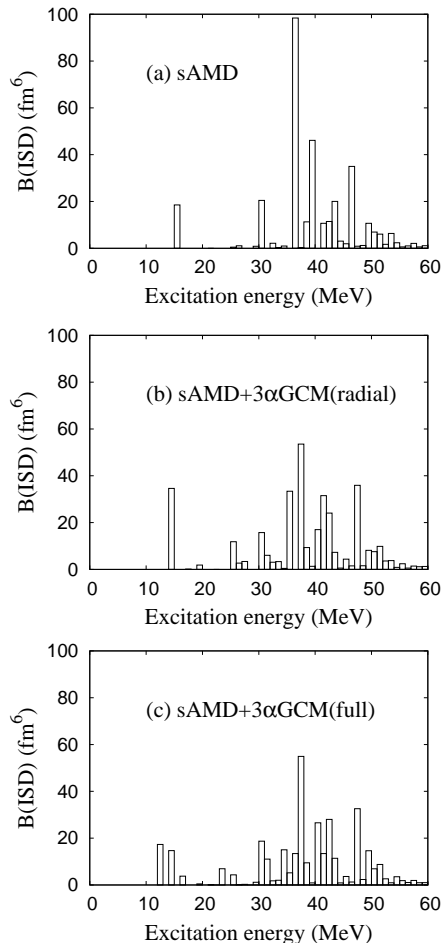


FIG. 5: The ISD strengths calculated by the sAMD, sAMD+3 α GCM(radial), and sAMD+3 α GCM(full). The sum of the strengths $B(\text{IS1})$ in each energy bin is shown.

state might come from the reaction model dependence in the DWBA analysis of nuclear scatterings. For the 0_3^+ state, the calculated strength exhausts 8% of the EWSR, which reasonably agrees to the experimental values, $6.9 \pm 0.9\%$ and $5 \pm 1\%$, for the 0_3^+ (10.3 MeV) measured by the (α, α') and $({}^6\text{Li}, {}^6\text{Li}')$ scatterings, respectively. The observed ISM strengths around $E = 10$ MeV were considered as a board 0_3^+ state at $E = 10.3$ MeV with a width of $\Gamma \sim 3$ MeV [9]. However, the recent experiment reported an indication that it contains two 0^+ states at $E = 9.04 \pm 0.09$ MeV with $\Gamma = 1.45 \pm 0.18$ and $E = 10.56 \pm 0.06$ MeV with $\Gamma = 1.42 \pm 0.08$ MeV [18]. It is likely that the ISM strengths for the 0_3^+ (10.3 MeV) reported in Refs. [9, 17] may contain the strengths for the two 0^+ states around $E = 10$ MeV above the 0_2^+ . Theoretically, the 3α orthogonal condition model ($3\alpha\text{OCM}$) calculations predicted two 0^+ states above the 0_2^+ state [31, 37], whereas the AMD, FMD, and microscopic 3α -cluster calculations predicted only one 0^+ state in this energy region [22, 25, 28, 33, 34, 36]. According to the $3\alpha\text{OCM}$ calculations, one of the two 0^+ states is a very broad state. The present framework is a bound state approximation, and therefore, it is not suitable to describe such the state strongly coupled by 3α continuum. If the missing 0^+ state comes to this energy region and mix with the 0_3^+ state, it could share a portion of the ISM strength for the 0_3^+ obtained in the present calculation. It means that the calculated ISM strength for the 0_3^+ exhausting 8% of the EWSR may correspond to the sum of the ISM strengths for possible 0^+ states in this energy region consistently to the experimental strengths evaluated by assuming a single 0^+ state at $E \sim 10$ MeV in Refs. [9, 17].

Let me look into the ISD strength distributions. As seen in Fig. 6(b), the high-energy ISD strengths corresponding to the ISGDR show a broad distribution mainly in $E = 30\text{--}55$ MeV. The structure of the broad ISGDR is qualitatively consistent with the observed ISD strengths shown in Fig. 6(d), however, the present calculation overestimates the observed peak energy of the ISGDR by about 10 MeV. The calculated ISD strengths in $E < 55$ MeV is 86% of the TEWS in the sAMD+3 α GCM(full), which is consistent with the observed ones in $E < 45$ MeV exhausting $78 \pm 9\%$ of

the EWSR [9].

The low-energy ISD strengths between $E = 10 - 20$ MeV exhaust 3.4% of the TEWS in the sAMD+3 α GCM(full). The calculated low-energy ISD strengths in ^{12}C is comparable to the observed low-energy ISD strengths (4% of the EWSR) in ^{16}O [48]. Compared with the sAMD result, the strength is enhanced by a factor 1.5 in the sAMD+3 α GCM(full) because of the cluster components in both the ground state and excited 1^- states. A couple of 1^- states contribute to the low-energy ISD strengths as seen in Fig. 6(b) for the sAMD+3 α GCM(full). The excitation energies of $E = 12.6$ MeV and $E = 14.8$ MeV of the 1_1^- and 1_2^- states obtained by the sAMD+3 α GCM(full) are consistent with those suggested by the 3 α -cluster calculation in Ref. [22]. The 1_1^- state is assigned to the experimentally known 1^- state at 10.84 MeV. For the 1_2^- state, there is no experimentally confirmed state. The calculated ISD strength for the 1_2^- state is 1.5% of the TEWS. The significant ISD strength suggests that the ISD excitations can be a good probe to experimentally observe the 1_2^- state. In the observed ISD strengths shown in Fig. 6(d), one can see a bump at $E \sim 15$ MeV, which can be a candidate of the 1_2^- state obtained in the present calculation. Unfortunately, it is difficult to extract the ISD strength for this state from the data because of the back ground ambiguity. The existence of the significant ISD strengths at $E \sim 15$ MeV is also supported by the measurement on (α, α') scattering at 386 MeV by Itoh *et al.* [57].

TABLE I: The energy weighted ISM and ISD strengths in the low-energy and high-energy regions calculated by the sAMD, sAMD+3 α GCM(radial), and sAMD+3 α GCM(full). The percentages of the ISM strengths in $E < 17$ MeV and $17 < E < 45$ MeV to the EWSR and those of the ISD strengths in $E < 20$ MeV and $20 < E < 55$ MeV to the TEWS are listed. The ISM TEWS (fm^4MeV), ISM EWSR (fm^4MeV), and ISD TEWS (fm^6MeV) are also shown.

	sAMD	sAMD+3 α GCM	
		(radial)	(full)
ISO			
TEWS	5.6×10^3	6.0×10^3	6.0×10^3
EWSR	5.8×10^3	6.0×10^3	6.0×10^3
$E < 17$	11%	26%	26%
$17 < E < 45$	0.64%	0.51%	50%
IS1			
TEWS	1.41×10^4	1.45×10^4	1.46×10^4
$E < 20$	2.1%	0.03.6%	3.4%
$20 < E < 55$	87%	83%	83%

TABLE II: The energy-weighted ISM strengths for the 0_2^+ and 0_3^+ states. The experimental data are those measured by (α, α') [9] and $(^6\text{Li}, ^6\text{Li}')$ [17] scatterings, and those evaluated by the E0 strengths measure by (e, e') [39, 40] assuming the mirror symmetry. The theoretical values are calculated by the sAMD+3 α GCM(full). The percentages to the EWSR are shown.

	cal. (e, e') [39]		(e, e') [40]	(α, α') [9]	$(^6\text{Li}, ^6\text{Li}')$ [17]
0_2^+	18	15	17	7.6 ± 0.9	9.5
0_3^+	8			6.9 ± 0.9	5 ± 1

IV. SUMMARY

I investigated the ISM and ISD excitations in ^{12}C with the sAMD+3 α GCM calculation. The small amplitude vibration modes are described by the coherent 1p-1h excitations expressed by small shift of single-nucleon Gaussian wave functions, whereas the large amplitude cluster modes are incorporated by superposing 3 α -cluster wave functions in the GCM. The coupling of the excitations in the intrinsic frame with the rotation and parity transformation is taken into account microscopically by the angular-momentum and parity projections. The present calculation describes the ISM and ISD excitations in a wide energy region covering the cluster excitations in the low-energy region and the giant resonances in the high-energy region.

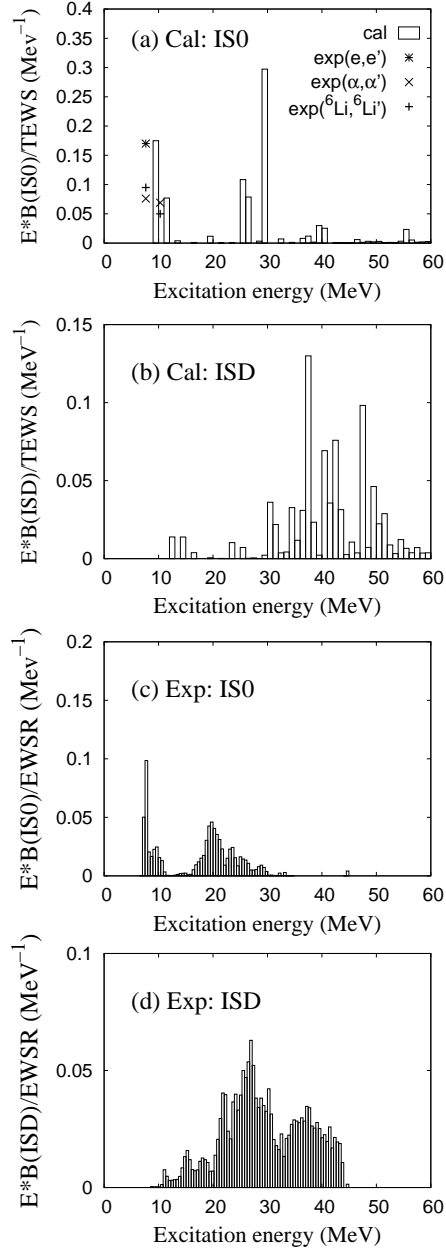


FIG. 6: The energy weighted ISM and ISD strength distributions calculated by the sAMD+3 α GCM(full) and those measured by (α, α') scatterings. For the calculated result, the ratio of the strengths in each energy bin to the TEWS is shown. The experimental data are those to the EWSR [9]. The panel (a) also shows the experimental values of the energy weighted ISM strengths in the unit of EWSR: the data for the 0_2^+ and 0_3^+ states measured by (α, α') [9] and $({}^6\text{Li}, {}^6\text{Li}')$ [17] scatterings, and that evaluated by the E0 strength measured by (e, e') scatterings [40] assuming the mirror symmetry.

In the calculated ISM strengths, the significant strengths corresponding to the cluster excitations are obtained in the low-energy region below the ISGMR. The low-energy ISM strength of the cluster mode is remarkably enhanced by the radial motion of α clusters, and it splits into two states by the angular motion of α clusters. The low-energy ISM strengths exhaust 26% of the EWSR, which is consistent with the experimental data for the 0^+ states at 7.65 MeV and 10.3 MeV measured by (e, e') , (α, α') , and $({}^6\text{Li}, {}^6\text{Li}')$ scatterings. The feature of the experimental ISM strength distributions which consists of the high-energy strengths of the ISGMR and the significant low-energy strengths are qualitatively described by the calculation, however, the quantitative description of the high-energy part is not satisfactory in the present result. The present calculation overestimates the centroid energy (21.9 ± 0.3 MeV) and

the strengths ($27\pm 5\%$ of the EWSR) of the ISGMR observed by (α, α') scatterings [9], and also fails to describe the experimental width of the ISGMR. The present model space is restricted only in the single-particle excitations written by shifted Gaussians and insufficient to describe the spreading width of the ISGMR.

Also in the calculated ISD strengths, the low-energy strength of the cluster mode is enhanced by the radial motion of α clusters, and it splits into a couple of states because of the angular motion of α clusters. Consequently, two 1^- states (the 1_1^- and 1_2^-) having the significant ISD strengths are obtained in $E = 10 - 15$ MeV. The lower state is assigned to the experimentally known 1^- state at 10.84 MeV. For the 1_2^- state, there is no experimentally confirmed state. The present calculation indicates that the ISD excitations can be a good probe to experimentally observe the 1_2^- state. In the experimental ISD strengths measured by (α, α') scatterings [9, 57], the bump observed at $E \sim 15$ MeV can be a candidate of the 1_2^- state obtained in the present calculation.

Acknowledgments

The author would like to thank Dr. Itoh and Dr. Kimura for fruitful discussions. The computational calculations of this work were performed by using the supercomputer in the Yukawa Institute for theoretical physics, Kyoto University. This work was supported by JSPS KAKENHI Grant Number 26400270.

-
- [1] D. H. Youngblood, C. M. Rozsa, J. M. Moss, D. R. Brown and J. D. Bronson, Phys. Rev. Lett. **39**, 1188 (1977).
 [2] H. P. Morsch, M. Rogge, P. Turek, C. Sukosd and C. Mayer-Boricke, Phys. Rev. C **20**, 1600 (1979).
 [3] C. M. Rozsa, D. H. Youngblood, J. D. Bronson, Y. W. Lui and U. Garg, Phys. Rev. C **21**, 1252 (1980).
 [4] D. H. Youngblood, P. Bogucki, J. D. Bronson, U. Garg, Y. W. Lui and C. M. Rozsa, Phys. Rev. C **23**, 1997 (1981).
 [5] D. H. Youngblood, Y.-W. Lui and H. L. Clark, Phys. Rev. C **57**, 2748 (1998).
 [6] D. H. Youngblood, Y.-W. Lui and H. L. Clark, Phys. Rev. C **60**, 014304 (1999).
 [7] Y.-W. Lui, H. L. Clark and D. H. Youngblood, Phys. Rev. C **64**, 064308 (2001).
 [8] D. H. Youngblood, Y.-W. Lui and H. L. Clark, Phys. Rev. C **63**, 067301 (2001) [Phys. Rev. C **64**, 049901 (2001)].
 [9] B. John, Y. Tokimoto, Y.-W. Lui, H. L. Clark, X. Chen and D. H. Youngblood, Phys. Rev. C **68**, 014305 (2003).
 [10] X. Chen, Y.-W. Lui, H. L. Clark, Y. Tokimoto and D. H. Youngblood, Phys. Rev. C **80**, 014312 (2009).
 [11] J. P. Blaizot, D. Gogny and B. Grammaticos, Nucl. Phys. A **265**, 315 (1976).
 [12] J. P. Blaizot, Phys. Rept. **64**, 171 (1980).
 [13] D. Vretenar, T. Niksic and P. Ring, Phys. Rev. C **68**, 024310 (2003).
 [14] G. Colo, N. Van Giai, J. Meyer, K. Bennaceur and P. Bonche, Phys. Rev. C **70**, 024307 (2004).
 [15] N. Paar, D. Vretenar, E. Khan and G. Colo, Rept. Prog. Phys. **70**, 691 (2007).
 [16] T. Yamada, Y. Funaki, T. Myo, H. Horiuchi, K. Ikeda, G. Ropke, P. Schuck and A. Tohsaki, Phys. Rev. C **85**, 034315 (2012).
 [17] W. Eyrich *et al.*, Phys. Rev. C **36**, 416 (1987).
 [18] M. Itoh *et al.*, Phys. Rev. C **84**, 054308 (2011).
 [19] M. Freer and H. O. U. Fynbo, Prog. Part. Nucl. Phys. **78**, 1 (2014).
 [20] Y. Fukushima and M. Kamimura, Proc. Int. Conf. on Nuclear Structure, Tokyo, 1977, edited by T. Marumori J. Phys. Soc. Jpn. **44**, 225 (1978).
 [21] M. Kamimura, Nucl. Phys. **A351**, 456 (1981).
 [22] E. Uegaki, S. Okabe, Y. Abe and H. Tanaka, Prog. Theor. Phys. **57**, 1262 (1977).
 [23] E. Uegaki, Y. Abe, S. Okabe and H. Tanaka, Prog. Theor. Phys. **62**, 1621 (1979).
 [24] P. Descouvemont and D. Baye, Phys. Rev. C **36**, 54 (1987).
 [25] Y. Kanada-En'yo, Phys. Rev. Lett. **81**, 5291 (1998).
 [26] A. Tohsaki, H. Horiuchi, P. Schuck, and G. Röpke, Phys. Rev. Lett. **87**, 192501 (2001).
 [27] Y. Funaki, A. Tohsaki, H. Horiuchi, P. Schuck and G. Ropke, Phys. Rev. C **67**, 051306 (2003).
 [28] T. Neff and H. Feldmeier, Nucl. Phys. **A738**, 357 (2004).
 [29] S. I. Fedotov, O. I. Kartavtsev, V. I. Kochkin and A. V. Malykh, Phys. Rev. C **70**, 014006 (2004).
 [30] C. Kurokawa and K. Kato, Nucl. Phys. **A738**, 455 (2004).
 [31] C. Kurokawa and K. Kato, Phys. Rev. C **71**, 021301 (2005).
 [32] I. Filikhin, V. M. Suslov and B. Vlahovic, J. Phys. G **31**, 1207 (2005).
 [33] Y. Kanada-En'yo, Prog. Theor. Phys. **117**, 655 (2007) [Erratum-ibid. **121**, 895 (2009)].
 [34] K. Arai, Phys. Rev. C **74**, 064311 (2006).
 [35] Y. Funaki, A. Tohsaki, H. Horiuchi, P. Schuck and G. Ropke, Eur. Phys. J. A **28**, 259 (2006).
 [36] M. Chernykh, H. Feldmeier, T. Neff, P. von Neumann-Cosel and A. Richter, Phys. Rev. Lett. **98**, 032501 (2007).
 [37] S. Ohtsubo, Y. Fukushima, M. Kamimura, and E. Hiyama, Prog. Theor. Exp. Phys. **2013**, 073D02 (2013).
 [38] S. Ishikawa, Phys. Rev. C **90**, no. 6, 061604 (2014).
 [39] P. Strehl, Z. Phys. **234**, 416 (1970).

- [40] M. Chernykh, H. Feldmeier, T. Neff, P. von Neumann-Cosel and A. Richter, *Phys. Rev. Lett.* **105**, 022501 (2010).
- [41] T. Kawabata, H. Akimune, H. Fujita, Y. Fujita, M. Fujiwara, K. Hara, K. Hatanaka and M. Itoh *et al.*, *Phys. Lett. B* **646**, 6 (2007).
- [42] Y. Kanada-En'yo, *Phys. Rev. C* **75**, 024302 (2007).
- [43] T. Wakasa, E. Ihara, K. Fujita, Y. Funaki, K. Hatanaka, H. Horiuchi, M. Itoh and J. Kamiya *et al.*, *Phys. Lett. B* **653**, 173 (2007).
- [44] T. Ichikawa, N. Itagaki, T. Kawabata, T. Kokalova and W. von Oertzen, *Phys. Rev. C* **83**, 061301 (2011).
- [45] T. Kawabata *et al.*, *Jour. Phys. Conf. Ser.* **436**, 012009 (2013).
- [46] Y. Chiba and M. Kimura, *Phys. Rev. C* **91**, no. 6, 061302 (2015).
- [47] H.P. Morsch, M. Rogge, P. Turek, and C. Mayer-B'oricke, *Phys. Rev. Lett.* **45**, 337 (1980).
- [48] M. N. Harakeh and A. E. L. Dieperink, *Phys. Rev. C* **23**, 2329 (1981).
- [49] G. Colo and G. N. Van, *Nucl. Phys. A* **731**, 15 (2004).
- [50] H. L. Clark, Y.-W. Lui and D. H. Youngblood, *Phys. Rev. C* **63**, 031301 (2001).
- [51] Y.-W. Lui, D. H. Youngblood, H. L. Clark, Y. Tokimoto and B. John, *Phys. Rev. C* **73**, 014314 (2006).
- [52] N. V. Giai and H. Sagawa, *Nucl. Phys.* **A371**, 1 (1981).
- [53] G. Colo, N. Van Giai, P. F. Bortignon and M. R. Quaglia, *Phys. Lett. B* **485**, 362 (2000).
- [54] D. Vretenar, N. Paar and P. Ring, *Phys. Rev. C* **65**, 021301 (2002).
- [55] P. Papakonstantinou, V. Y. Ponomarev, R. Roth and J. Wambach, *Eur. Phys. J. A* **47**, 14 (2011).
- [56] T.D. Poelheken, S.K.B. Hesmondhalgh 1, H.J. Hofmann, A. van der Woude, *Phys. Letts. B* **278**, 423 (1992).
- [57] M. Itoh *et al.*, private communication (2015).
- [58] Z. Ma, N. Van Giai, H. Toki and M. L'Huillier, *Phys. Rev. C* **55**, 2385 (1997).
- [59] A. Lovato, S. Gandolfi, R. Butler, J. Carlson, E. Lusk, S. C. Pieper and R. Schiavilla, *Phys. Rev. Lett.* **111**, no. 9, 092501 (2013).
- [60] Y. Kanada-En'yo, H. Horiuchi and A. Ono, *Phys. Rev. C* **52**, 628 (1995).
- [61] Y. Kanada-En'yo and H. Horiuchi, *Phys. Rev. C* **52**, 647 (1995).
- [62] Y. Kanada-En'yo and H. Horiuchi, *Prog. Theor. Phys. Suppl.* **142**, 205 (2001).
- [63] Y. Kanada-En'yo, M. Kimura and A. Ono, *PTEP* **2012** 01A202 (2012).
- [64] Y. Kanada-En'yo, *Phys. Rev. C* **89**, 024302 (2014).
- [65] Y. Kanada-En'yo, arXiv:1511.08530 [nucl-th].
- [66] Y. Kanada-En'yo and M. Kimura, *Phys. Rev. C* **72**, 064301 (2005).
- [67] T. Furuta, K. H. O. Hasnaoui, F. Gulminelli, C. Leclercq and A. Ono, *Phys. Rev. C* **82** (2010) 034307.
- [68] A. Ono, H. Horiuchi, T. Maruyama and A. Ohnishi, *Phys. Rev. Lett.* **68**, 2898 (1992).
- [69] A. Ono, H. Horiuchi, T. Maruyama and A. Ohnishi, *Prog. Theor. Phys.* **87**, 1185 (1992).
- [70] H. Feldmeier, K. Bieler and J. Schnack, *Nucl. Phys. A* **586**, 493 (1995).
- [71] T. Neff and H. Feldmeier, *Nucl. Phys. A* **713**, 311 (2003).
- [72] D. M. Brink, *Proc. Int. School of Physics Enrico Fermi, Course 36*, Varenna, ed. C. Bloch (Academic Press, New York, 1966).
- [73] T. Ando, K. Ikeda, and A. Tohsaki, *Prog. Theor. Phys.* **64**, 1608 (1980).
- [74] R. Tamagaki, *Prog. Theor. Phys.* **39**, 91 (1968).
- [75] N. Yamaguchi, T. Kasahara, S. Nagata, and Y. Akaishi, *Prog. Theor. Phys.* **62**, 1018 (1979).
- [76] I. Angeli and K. P. Marinova, *At. Data Nucl. Data Tables* **99**, 69 (2013).